01 Jan 1991

Analysis Of Shear Banding In Plane Strain Compression Of A Bimetallic Thermally Softening Viscoplastic Body Containing An Elliptical Void

Z. G. Zhu

R. C. Batra
Missouri University of Science and Technology

Recommended Citation

Z. G. Zhu and R. C. Batra, "Analysis Of Shear Banding In Plane Strain Compression Of A Bimetallic Thermally Softening Viscoplastic Body Containing An Elliptical Void," *Journal of Engineering Materials and Technology, Transactions of the ASME*, vol. 113, no. 4, pp. 382 - 395, American Society of Mechanical Engineers, Jan 1991.
The definitive version is available at https://doi.org/10.1115/1.2904116

Analysis of Shear Banding in Plane Strain Compression of a Bimetallic Thermally Softening Viscoplastic Body Containing an Elliptical Void

Z. G. Zhu

R. C. Batra

Department of Mechanical and Aerospace Engineering and Engineering Mechanics, University of Missouri-Rolla, Rolla, MO 65401-0249

We study plane strain thermomechanical deformations of a prismatic viscoplastic body of square cross-section and deformed at a nominal strain-rate of 5000 s^{-1}. The body has two thin layers placed symmetrically about the horizontal centroidal axis and an elliptical void at the center. The major axis of the void coincides with the vertical centroidal axis and also with the direction of loading. The layer material differs from that of the body in only the value of the yield stress in a quasistatic simple compression test. The yield stress for the layer material is taken to be either one-fifth or five times that of the matrix material. The deformations are assumed to be symmetrical about the vertical and horizontal centroidal axes. It is found that in each case shear bands initiate from points on the traction free edges where the matrix/layer interfaces intersect them and propagate into the softer material. For the soft layer these bands initially merge into one and propagate horizontally. Subsequently, each of these bands bifurcates into two which propagate into the matrix material along the direction of the maximum shear stress. There is minimal interaction between these bands and those initiating from points slightly away from the void tips. These latter bands pass through the soft layer rather easily. When the layer material is harder than the matrix material, the material in the first quadrant is eventually divided into five subregions each of which is deforming virtually rigidly and the velocity suffers a sharp jump across the boundaries between these regions.

Introduction

Adiabatic shear bands are narrow regions of intense plastic deformation that form during high strain-rate processes, such as shock loading, ballistic penetration, metal forming, and machining. As these bands generally precede material fracture, a knowledge of factors that inhibit or enhanced their growth is essential to the production of durable materials and more efficient manufacturing processes. These bands form in both ferrous and nonferrous alloys.

Johnson (1987) has recently pointed out that Tresca (1878) and Massey (1921) observed hot lines, now referred to as adiabatic shear bands, during the forging of platinum. Both Tresca and Massey stated that these were the lines of greatest sliding, and also therefore the zones of greatest development of heat. Subsequently, Zener and Hollomon (1944) observed 32μm wide shear bands during the punching of a hole in a 0.25 percent C low alloy steel plate and added that heating caused by the plastic deformation of the material made it softer and the material became unstable when this thermal softening equalled the combined effects of strain and strain-rate hardening. Recent experimental findings of Marchand and Duffy (1988) on HY-100 steel and of Marchand, Cho and Duffy (1989) on AISI 1018 cold-rolled steel indicate that the shear strain localization phenomenon consists of three stages. In the first stage, the deformation stays homogeneous. The stage two, stipulated to initiate when the shear stress attains its peak value, involves nonhomogeneous deformations of the block. In stage three, the shear stress drops precipitously and the severely deforming region narrows down considerably. Thus the stability criterion (Recht, 1964; Clifton, 1980) based on the stress attaining a maximum value will predict the initiation of the stage two rather than the beginning of the intense localization of the deformation.

Wulf (1978) has reported experimental observations of adiabatic shear bands in high strain rate (2000 to 25,000 s^{-1}) compression of 7039 aluminum armour. He found that the cross-section of the cylindrical specimens changed from circular to elliptical after the compression test, and adiabatic shear bands formed in the specimens which subsequently failed by

Contributed by the Materials Division for publication in the JOURNAL OF ENGINEERING MATERIALS AND TECHNOLOGY. Manuscript received by the Materials Division August 8, 1990; revised manuscript received November 10, 1990.

crack propagation along the dominant band. Further references to the analytical, numerical and experimental work on shear banding may be found in two recent books (Dodd and Bai, 1987; Semiatin and Jonas, 1984) and the recent paper by Shawki and Clifton (1989). Shawki and Clifton have classified the proposed mechanisms for the shear band formation into two main categories: (i) mechanisms associated with shear localization during the quasi-static, isothermal deformations of rate-independent materials, and (ii) mechanisms associated with shear localization during the dynamic, adiabatic deformations of rate-sensitive materials. In category (i), shear banding is viewed as a material instability that takes place due to the loss of ellipticity of the rate equations of continuing equilibrium. A summary of the work related to shear strain localization in quasistatic and isothermal plastic deformations done through 1983 has been provided by Needleman and Tvergaard (1984). Herein, we are primarily interested in analyzing the localization phenomenon under high strain-rate conditions and hence the present work belongs to category (ii).

Many of the works on shear banding referred to above have involved analyzing simple shearing deformations of a viscoplastic block containing a material inhomogeneity. Recently, LeMonds and Needleman (1986), Needleman (1989), Anand et al. (1988), Zbib and Aifantis (1988), Batra and Liu (1989, 1990), Zhu and Batra (1990), Batra and Zhu (1990), and Batra and Zhang (1990) have studied the phenomenon of shear banding in plane strain deformations of a viscoplastic solid. Whereas Needleman studied a purely mechanical problem, other works have treated a coupled thermomechanical problem. LeMonds and Needleman, Zbib and Aifantis, and Anand et al. neglected the effect of inertia forces on the ensuing deformations of the body. These investigations have employed different constitutive relations, different techniques to integrate the stiff set of governing partial differential equations, and have generally assumed that the entire body or the portion of the body whose deformations were analyzed had only one defect in it. The prismatic body whose plane strain thermomechanical deformations are studied herein is of a square cross-section and has two thin layers made of a viscoplastic material different from that of the body and placed symmetrically about and parallel to the centroidal horizontal axis. These horizontal layers may be thought of as representing planes of chemical inhomogeneity. Also, there is an ellipsoidal void with its major axis aligned along the vertical centroidal axis of the cross-section. The centers of the void and the cross-section coincide with each other. The voids can form during manufacturing. However, the symmetrical situation considered herein is to simplify the problem. For the present problem, the vertices of the ellipsoidal void on its major axis and the points on the free edges where the thin layer and the matrix materials meet act as nuclei for the initiation of shear bands. It thus becomes an interesting exercise to study the initiation and growth of various bands and the interaction, if any, amongst them. We account for the effect of inertia forces, strain-rate sensitivity of the materials, thermal softening effects, heat conduction, and the heat generated due to plastic working.

Formulation of the Problem

Figure 1 depicts the cross-section of the prismatic body, and the relative dimensions of the ellipsoidal void and the two thin layers. It is assumed that the body is loaded along the vertical axis, plane strain state of deformation prevails, and that the deformations are symmetrical about the two centroidal axes. Thus the deformations of the material in the first quadrant are analyzed. We use a fixed set of rectangular cartesian coordinate axes and the referential description of motion to describe the thermomechanical deformations of the body. The governing equations are:

balance of mass: $(\rho J)^{\cdot} = 0$, (2.1)

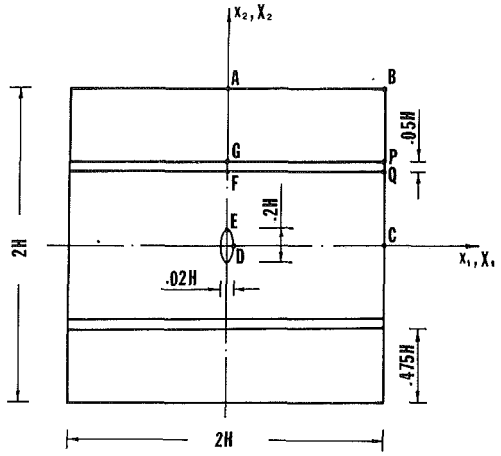

Fig. 1 Cross-section of the prismatic body studied

balance of linear momentum: $\rho_0 \dot{v}_i = T_{i\alpha,\alpha}$, (2.2)

balance of moment of momentum: $T_{i\alpha} x_{j,\alpha} = T_{j\alpha} x_{i,\alpha}$, (2.3)

balance of internal energy: $\rho_0 \dot{e} = -Q_{\alpha,\alpha} + T_{i,\alpha} v_{i,\alpha}$, (2.4)

where

$$T_{i\alpha} = (\rho_0/\rho)\sigma_{ij} X_{\alpha,j},\ \sigma_{ij} = -B(\rho/\rho_0 - 1)\delta_{ij} + 2\mu D_{ij}, \quad (2.5)$$

$$2\mu = [\sigma_0/\sqrt{3}I](1 + bI)^m (1 - \nu\theta), \quad (2.6)$$

$$I^2 = (1/2)\overline{D}_{ij}\overline{D}_{ij}, \quad (2.7)$$

$$\overline{D}_{ij} = D_{ij} - 1/3 D_{kk}\delta_{ij}, \quad (2.8)$$

$$Q_\alpha = (\rho_0/\rho) q_i X_{\alpha,i},\ q_i = -k\theta_{,i}, \quad (2.9)$$

$$\dot{e} = c\dot{\theta} + B(\rho/\rho_0 - 1)\dot{\rho}/\rho^2. \quad (2.10)$$

In these equations x_i gives the position at time t of the material particle X_α, $v_i = \dot{x}_i$ is its velocity in the x_i-direction, ρ is its present mass density, ρ_0 its mass density in the reference configuration, $J = \det[x_{i,\alpha}]$, $x_{i,\alpha} = \partial x_i/\partial X_\alpha$, $T_{i\alpha}$ is the first Piola-Kirchoff stress tensor, σ_{ij} is the Cauchy stress tensor, e is the specific internal energy, Q_α is the heat flux measured per unit area in the reference configuration, $\underset{\sim}{D}$ is the strain-rate tensor and $\overline{\underset{\sim}{D}}$ is its deviatoric part, a superimposed dot indicates material time derivative, a comma followed by index $\alpha(j)$ implies partial differentiation with respect to $X_\alpha(x_j)$, and a repeated index implies summation over the range (1,2) of the index. In the constitutive relations (2.5), (2.9) and (2.10), the material parameter B represents the bulk modulus, σ_0 is the yield stress in a quasistatic simple compression test, parameters b and m characterize the strain-rate sensitivity of the material, ν describes its thermal softening, θ equals the temperature change of a material particle from that in the reference configuration, k is the constant thermal conductivity and c is the constant specific heat. Here we have not considered the stresses caused by the thermal expansion.

The foregoing equations hold in regions occupied by the matrix and the layers. The values of material parameters for the matrix and the layer materials are the same except that either

$$\sigma_0^{\text{layer}} = 5\sigma_0^{\text{matrix}}, \quad (2.11a)$$

or

$$\sigma_0^{\text{layer}} = (1/5)\sigma_0^{\text{matrix}}. \quad (2.11b)$$

In terms of the deviatoric stress s defined by

$$\underset{\sim}{s} = \underset{\sim}{\sigma} + [B(\rho/\rho_0 - 1) - (2\mu/3) tr \underset{\sim}{D}]\underset{\sim}{1}, \quad (2.12a)$$

$$= 2\mu \overline{\underset{\sim}{D}}, \quad (2.12b)$$

equations (2.12), (2.5) and (2.6) give

$$(1/2\ tr\ \underset{\sim}{s}^2)^{1/2} = (\sigma_0/\sqrt{3})(1 - \nu\theta)(1 + bI)^m. \quad (2.13)$$

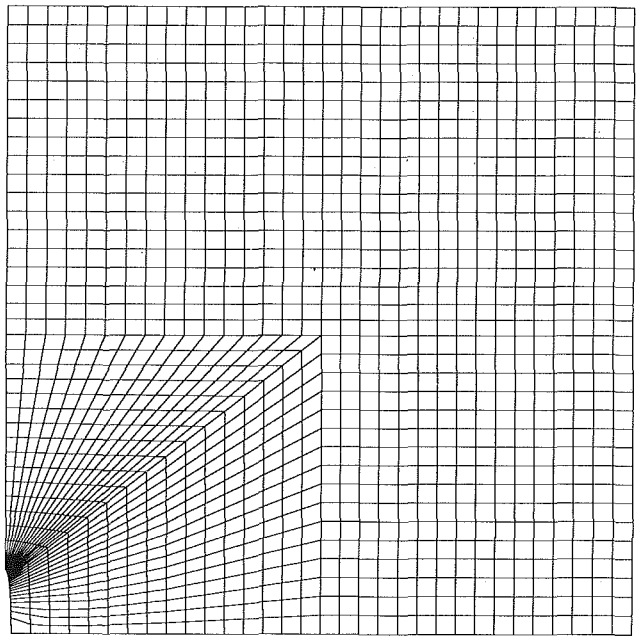

Fig. 2 Finite element discretization of the domain

We assume that the body is initially at rest at a uniform temperature, has a constant mass density and is initially stress free. That is

$$\rho(\underset{\sim}{x}, o)=1,\ \underset{\sim}{v}(\underset{\sim}{x}, o)=\underset{\sim}{o},\ \theta(x, o)=0. \tag{2.14}$$

For the material in the first quadrant, we impose the following boundary conditions.

$$v_2=-h(t),\ T_{12}=0 \text{ and } Q_2=0, \text{ on the top surface } AB, \tag{2.15}$$

$$T_{11}=0,\ T_{21}=0 \text{ and } Q_1=0, \text{ on the right surface } BC, \tag{2.16}$$

$$v_2=0,\ T_{12}=0 \text{ and } Q_2=0, \text{ on the bottom surface } CD, \tag{2.17}$$

$$T_{i\alpha}N_\alpha=0,\ Q_\alpha N_\alpha=0, \text{ on the void surface } DE, \tag{2.18}$$

$$v_1=0,\ T_{21}=0 \text{ and } Q_1=0, \text{ on the left surface } EA. \tag{2.19}$$

That is, the top surface is moving downward with a speed $h(t)$, contact between it and the loading device is smooth, the right surface is traction free, and the entire boundary is thermally insulated. If at any time during the deformations of the body, any point on the void surface touches the vertical axis, the boundary condition on it is changed to (2.19). The boundary conditions (2.17) and (2.18) reflect the presumed symmetry of deformations about the x_1 and x_2 axes. For the loading function $h(t)$ we take

$$\begin{aligned} h(t) &= v_0\, t/t_r,\ 0\le t\le t_r, \\ &= v_0 \qquad t>t_r. \end{aligned} \tag{2.20}$$

The steady speed v_0 of the top surface of the block is reached in time t_r.

The matrix and the layer are assumed to be perfectly bonded. Thus at the common interfaces between them, the velocity field, surface tractions, the temperature and the normal component of the heat flux are assumed to be continuous.

Computational Considerations

We use the updated Lagrangian method (e.g., see Bathe 1982) to find an approximate solution of the problem. That is, to find the deformations of the body at time $t+\Delta t$, its configuration at time t is taken as the reference configuration. The coupled nonlinear partial differential equations obtained by substituting for $\underset{\sim}{T}$, Q and e from (2.5) through (2.10) into the balance laws (2.2) and (2.4), and the balance of mass (2.1) are to be solved for ρ, $\underset{\sim}{v}$ and θ. These equations are first reduced to a set of coupled nonlinear ordinary differential equations by using the Galerkin approximation (Bathe (1982)) and the lumped mass matrix. These equations are integrated by using the Gear method (1971) for stiff differential equations. We used the subroutine LSODE taken from the package ODEPACK, developed by Hindmarsh (1983), and employed the option of using the full Jacobian matrix. The subroutine adjusts the time step adaptively until a solution of the coupled nonlinear ordinary differential equations has been computed to the desired accuracy. The finite element code developed by Batra and Liu (1989) was modified to study the present problem.

Figure 2 shows the discretization of the stress free reference configuration into 4-noded isoparametric quadrilateral elements used to analyze the problem. Note that nodal coordinates are updated after each time increment. Thus, the spatial domain occupied by the body and the shapes of these elements vary with time. At each node, the mass density, two components of the velocity and the temperature are unknown.

Discussion of Results

In order to compute results, we used the following values of various material and geometric parameters.

$$\begin{aligned} &b=10000 \text{ s},\ \sigma_0=333 \text{ MPa},\ k=49.22\ W\,m^{-1}\,{}^\circ C^{-1}, \\ &m=0.025, \\ &c=473\ J\,\text{Kg}^{-1}\,{}^\circ\text{C}^{-1},\ \rho_0=7860\ \text{Kg}\ m^{-3}, \\ &\text{B}=128 \text{ GPa}, \\ &H=5 \text{ mm},\ v_0=25\ m\ \text{s}^{-1},\ \nu=0.0025\ {}^\circ C^{-1}. \end{aligned} \tag{3.1}$$

Thus the average applied strain-rate $\dot\gamma_{\text{avg}}$ equals 5000 s^{-1}, the reference temperature $\theta \equiv \sigma_0/(\rho_0 c) = 89.6°C$, and $\delta = \rho_0 v_0^2/\sigma_0 = 0.015$. The nondimensional number δ signifies the effect of inertia forces relative to the flow stress of the material. For the simple shearing problem, Batra (1988) noted that the inertia forces play a noticeable role when $\delta = 0.004$. Thus for the present problem, the inertia forces will very likely play a significant role.

Results are discussed below in terms of the nondimensional variables indicated in equation (3.2) by a superimposed bar.

$$\begin{aligned} &\overline{\underset{\sim}{s}}=\underset{\sim}{s}/\sigma_0,\ \bar\theta=\theta/\theta_0,\ \overline{\underset{\sim}{x}}=\underset{\sim}{x}/H, \\ &s_e\equiv(1/2\ tr\ \overline{\underset{\sim}{s}}^2)^{1/2}. \end{aligned} \tag{3.2}$$

Henceforth, we drop the superimposed bars. We call s_e the effective stress at a point. To measure the deformations of a point, we use the maximum principal logarithmic strain ϵ defined as

$$\epsilon=ln\ \lambda_1\simeq -ln\ \lambda_2, \tag{3.3}$$

where λ_1^2 and λ_2^2 are eigenvalues of the right Cauchy-Green tensor $C_{\alpha\beta}=x_{i,\alpha}x_{i,\beta}$ or the left Cauchy-Green tensor $B_{ij}=x_{i,\alpha}x_{j,\alpha}$. The second equality in equation (3.3) holds because the deformations are nearly isochoric.

4.1 Layer Material Softer than the Matrix Material. In order to decipher where shear bands form and their directions of propagation, we plot the evolution of the maximum principal logarithmic strain ϵ at several points surrounding the void tip and at points near the common interfaces between the layer and the matrix material. Figs. 3(*a*), 3(*b*), 3(*c*), 3(*d*), and 3(*e*) depict the growth of ϵ at 23 points in the vicinity of the ellipsoidal void and also at point 50 in the matrix that is far removed from the void and the layer/matrix interfaces. The approximate locations of these points, except that of point 50, are shown in Fig. 3(*b*), and coordinates of these points are

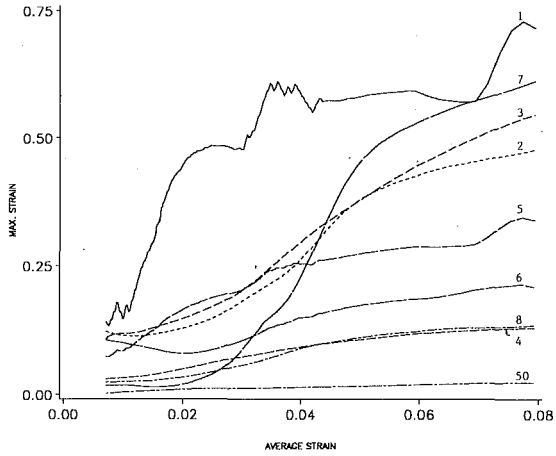

Fig. 3*(a)* Evolution of the maximum principal logarithmic strain ϵ at points 1, 2, 3, 4, 5, 6, 7, 8 near the void tip and point 50 in the matrix *when the layer material is weaker than the matrix material.*

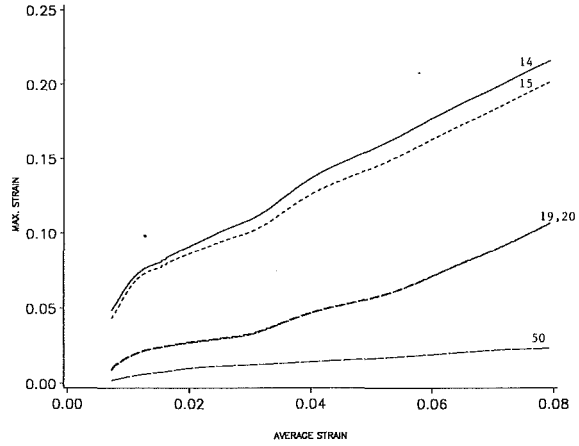

Fig. 3*(d)* Evolution of ϵ at points 14, 15, 19, 20 and 50 when $\sigma_0^{layer} = 0.2\ \sigma_0^{matrix}$.

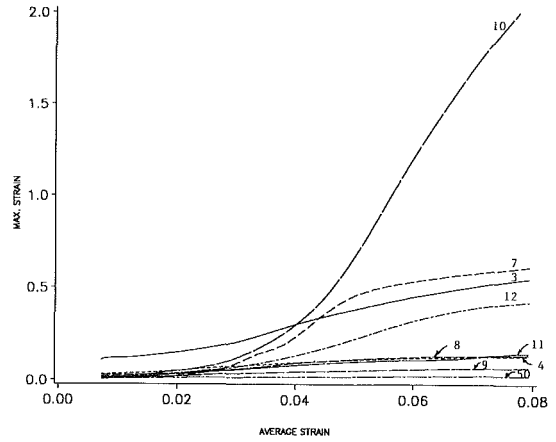

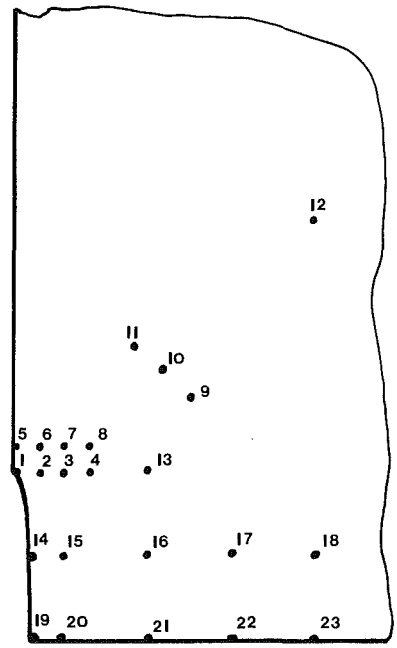

Fig. 3*(b)* Evolution of ϵ at points 3, 4, 7, 8, 9, 10, 11, 12 near the void tip and point 50 in the matrix when $\sigma_0^{layer} = 0.2\ \sigma_0^{matrix}$. Also shown in the figure is the approximate location of points where the evolution of ϵ is plotted in Figs. 3*(a)* through 3*(e)*. The coordinates of these points are: 1(0.1 E-04, 0.1), 2(0.015, 0.1), 3(0.03, 0.1), 4(0.045, 0.1), 5(0.1 E-04, 0.115), 6(0.015, 0.115), 7(0.03, 0.115), 8(0.045, 0.115), 9(0.1077, 0.1423), 10(0.09, 0.16), 11(0.0723, 0.1776), 12(0.18, 0.25), 13(0.08, 0.1), 14(0.01, 0.05), 15(0.03, 0.5), 16(0.08, 0.05), 17(0.13, 0.05), 18(0.18, 0.05), 19(0.01, 0.1 E-04), 20(0.03, 0.1 E-04), 21(0.08, 0.1 E-04), 22(0.13, 0.1 E-04), 23(0.18, 0.1 E-04), 50 (0.8, 0.1 E-02)

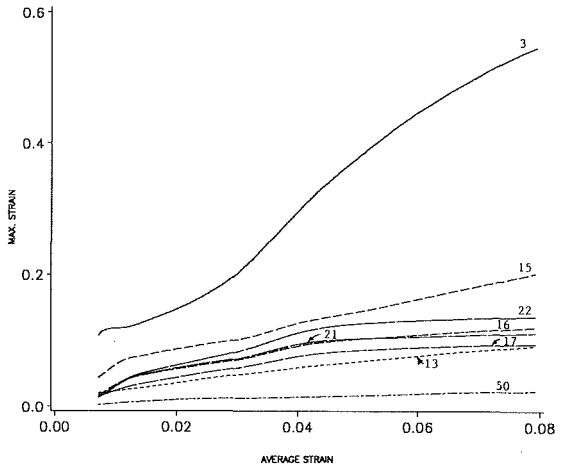

Fig. 3*(c)* Evolution of ϵ at points 3, 13, 15, 16, 17, 21, 22 and 50 when $\sigma_0^{layer} = 0.2\ \sigma_0^{matrix}$.

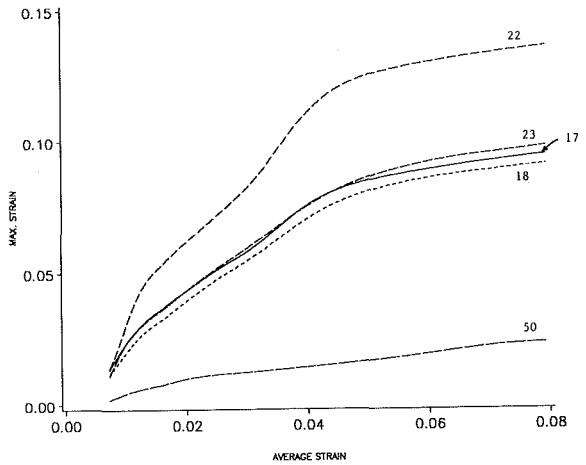

Fig. 3*(e)* Evolution of ϵ at points 17, 18, 22, 23 and 50 when $\sigma_0^{layer} = 0.2\ \sigma_0^{matrix}$.

given in the caption to Fig. 3(*b*). Note that the vertical scale in each of Figs. 3(*a*) through 3(*e*) is different. Except for point 1 near the void tip, ϵ evolves smoothly at all other points considered. Initially because of singular deformations near the void tip, the strain ϵ there rises sharply. The severe deformations near point 1 raise the temperature of the material surrounding that point and make is softer. However, the surrounding relatively harder material constrains the deformations of the material enclosing point 1 resulting in a redistribution of the deformations. The plotted results indicate that the material region enclosing points 1, 2, 3, 7, 10, and 12 is deforming more severely than the rest of the material surrounding the void. However, the nucleus of the band seems to be point 10 where, judging from the rate of growth of ϵ, a shear band initiates at an average strain of approximately 0.026 and propagates toward point 12. The temperature rise and the evolution of the effective stress at numerous points, including points 10 and 12, are plotted in Figs. 4(*a*) and 4(*b*), respectively. The effective stress at points 10 and 12 drops rather gradually in consonance with the slow rate of increase of temperature at these two points. We note that for the one-dimensional simple shearing problem, the temperature rises rapidly and the shear stress drops precipitously at the band center, e.g., see Batra and Kim (1990a, 1990b). The contours of ϵ plotted in the reference configuration, and at six different values of the average strain and depicted in Figs. 5(*a*) through 5(*f*) together with the plots of ϵ at numerous points included in Figs. 3(*a*) through 3(*e*) suggest that severe deformations initiating from point 1 near the void tip propagate horizontally to point 3 where they get bifurcated into two bands, each propagating in the ± 45 deg direction. The band propagating towards the horizonal axis arrives there at the same time as does the one initiating from the other void tip. For sometime then we have two bands propagating parallel to each other which eventually merge to give a wide zone of material undergoing large deformations. By examining closely the contours of ϵ, it is clear that only one shear band with center around point 10 propagates in a direction that makes an angle of nearly 45 deg with the horizontal. As pointed out by Needleman (1989), and Zhu and Batra (1991), contours of different values of ϵ propagate at different speeds.

In an attempt to elucidate upon what happens when contours of ϵ meet the matrix/layer interface, we have plotted in Figs. 6(*a*) through 6(*d*) the evolution of ϵ and θ at several points in the region where the line joining points 10 and 12 intersects the layer. The approximate location of these points is shown in Fig. 6(*a*). Points 24 and 34 in the matrix are on the line joining points 10 and 12; points 27 and 31 in the soft layer adjoin points 24 and 34 in the matrix. The higher temperature at points 24, 25, 34, and 35 suggests that the matrix material surrounding these points has undergone larger deformations as compared to the adjoining matrix material. Note that the rate of increase of temperature and ϵ at these four points as well as at points 27, 28, 31, and 32 in the layer is increasing. Since the yield stress in a quasistatic compression test for the layer material is one-fifth that of the matrix material, for the same applied load the strain in the layer should be more than that in the matrix. However, because of the larger temperature rise at matrix points, they have softened more than the nearby layer particles. The contours of ϵ plotted in Fig. 5 and the evolution of ϵ at several points plotted in Fig. 6 suggest that the band on meeting the matrix/layer interface is deflected a little to the right and passes through the layer rather easily.

The contours of ϵ depicted in Fig. 5 also reveal that shear bands initiate from points on the right traction free edge where the matrix/layer interfaces intersect it. Because the layer material is softer and its thickness quite small, these bands merge into one band that initially propagates horizontally into the layer. When the matrix material has softened somewhat due to the rise in its temperature, the horizontally propagating band

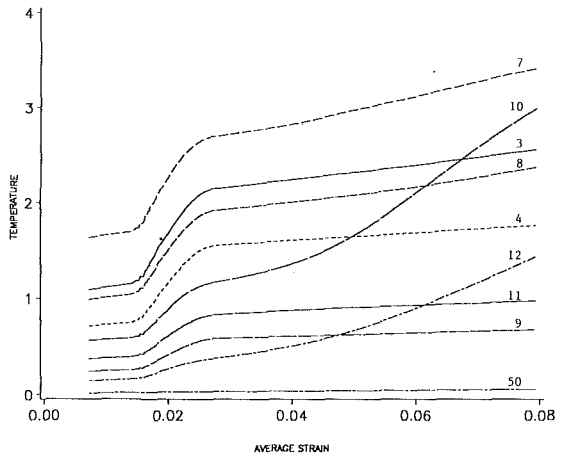

Fig. 4(*a*) Evolution of the temperature rise θ at points 3, 4, 7, 8, 9, 10, 11, 12 and 50 when $\sigma_0^{layer} = 0.2\ \sigma_0^{matrix}$.

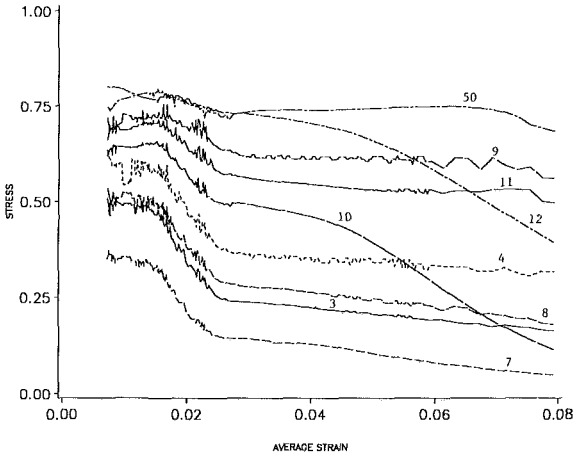

Fig. 4(*b*) Evolution of the effective stress at points 3, 4, 7, 8, 9, 10, 11, 12 and 50 when $\sigma_0^{layer} = 0.2\ \sigma_0^{matrix}$.

bifurcates into two bands that propagate into the matrix along ± 45 deg directions. The band propagating into the matrix material above the layer has more severe deformations associated with it than the one propagating into the matrix material below the layer. In order to evidence this, we have plotted in Figs. 7(*a*) and 7(*b*) the evolution of ϵ at several layer and matrix points near the upper matrix/layer interface. The approximate location of these points is depicted in Fig. 7(*c*), and their coordinates are given in the figure caption. Whereas curves of ϵ versus the average strain at points 10 and 12 near the void tip are concave upwards, those for points in Figs. 7(*a*) and 7(*b*) are concave downwards. Thus the values of ϵ at matrix and layer points considered for Figs. 7(*a*) and 7(*b*) will very likely reach a plateau. The strain at points in the layer is more because its material is weaker than the matrix material. These plots suggest that the band initiating from point 36 propagates horizontally into the layer to point 38 where it bifurcates into the matrix material and propagates along the line joining points 43, 47 and 49. Note that points 38 and 43 are on the opposite side of the matrix/layer interface.

Figure 8 shows the distribution of v_2 and the effective stress at an average strain of 0.0601. The sharp jump in the value of v_2 across a shear band supports the assertion by Tresca (1878) and Massey (1921) that the tangential velocity is discontinuous across a shear band. In our work, the velocity field is forced to be continuous throughout the region. The drop in the effective stress in a narrow region near the void tip indicates that the intense band has formed only there.

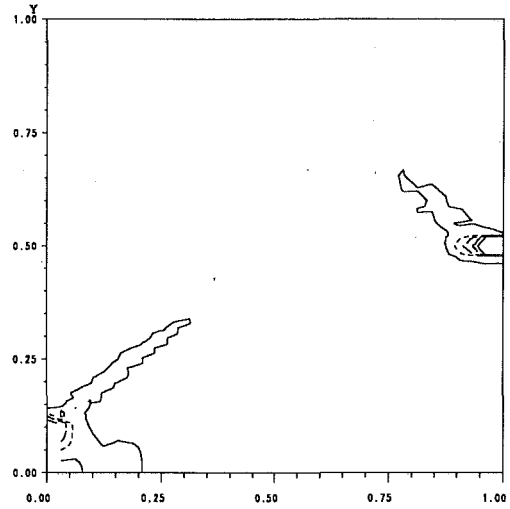

Fig. 5*(a)*

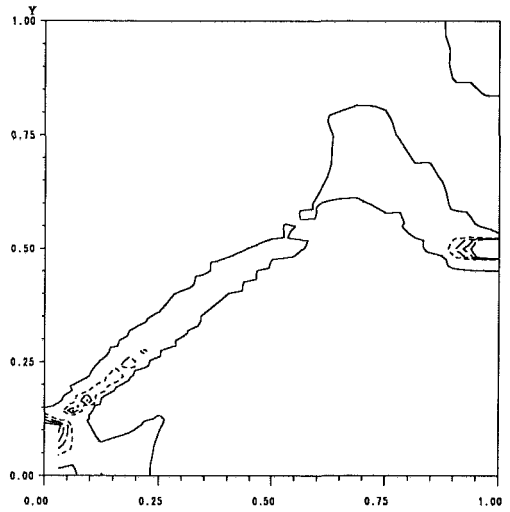

Fig. 5*(b)*

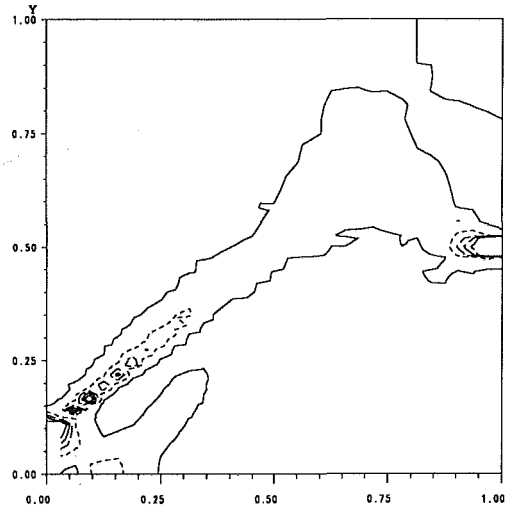

Fig. 5*(c)*

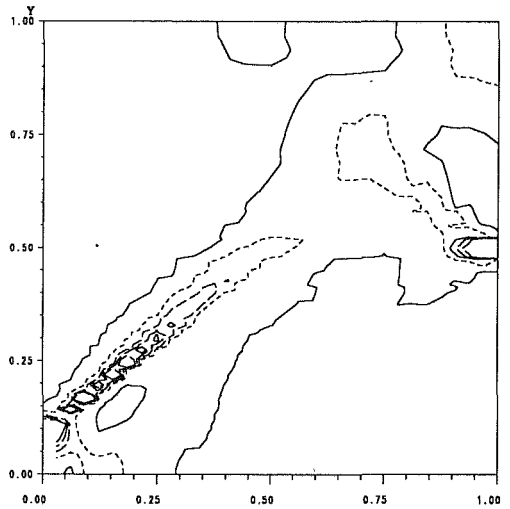

Fig. 5*(d)*

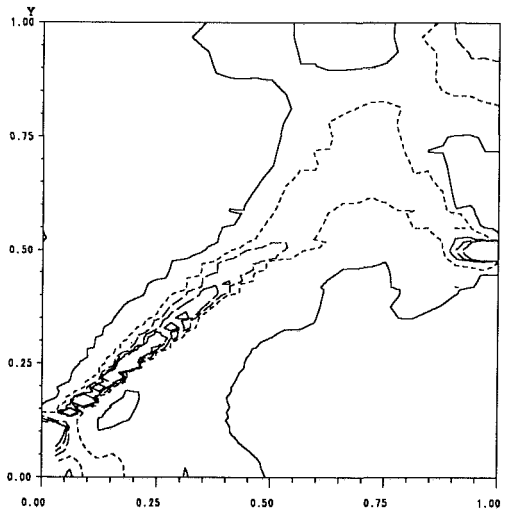

Fig. 5*(e)*

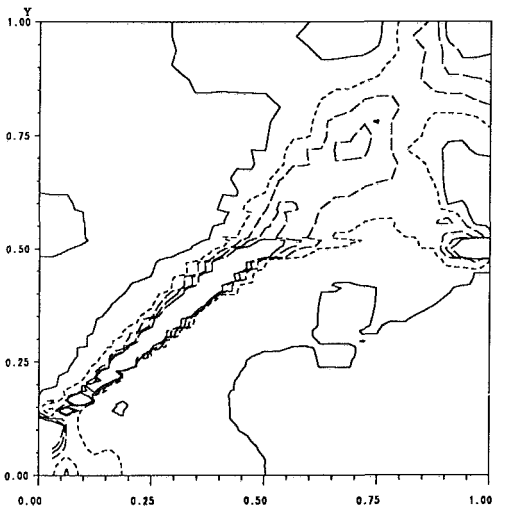

Fig. 5*(f)*

Fig. 5 Contours of ϵ at different valuesof the average strain when $\sigma_0^{layer} = 0.2\ \sigma_0^{matrix}$. ——— 0.05, · · · · · 0.10, — — — — 0.15, ——— ——— ——— 0.20, ——— · ——— · 0.25. *(a)* $\gamma_{avg} = 0.029$, *(b)* $\gamma_{avg} = 0.036$, *(c)* $\gamma_{avg} = 0.0421$, *(d)* $\gamma_{avg} = 0.054$, *(e)* $\gamma_{avg} = 0.061$, *(f)* $\gamma_{avg} = 0.079$

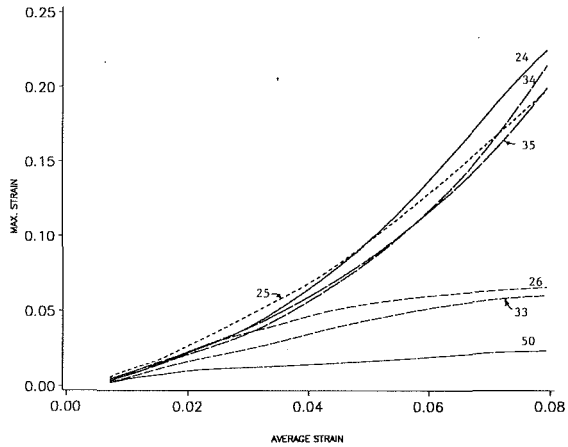

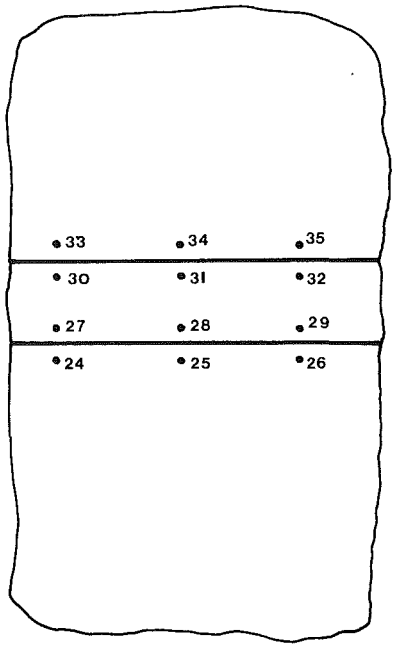

Fig. 6*(a)* **Evolution of ϵ at matrix points 24, 25, 26, 33, 34 and 35 near the matrix/layer interfaces and point 50 in the matrix when $\sigma_0^{layer} = 0.2\sigma_0^{matrix}$. The insert shows the approximate location of points where the evolution of ϵ and θ is plotted in Figs. 6*(a)* through 6*(d)*. The coordinates of these points are: 24(0.395, 0.465), 25(0.47, 0.465), 26(0.54, 0.465), 27(0.395, 0.485), 28(0.47, 0.485), 29(0.54, 0.485), 30(0.395, 0.515), 31(0.47, 0.515), 32(0.54, 0.515), 33(0.395, 0.535), 34(0.47, 0.535), 35(0.54, 0.535), 51(0.1, 0.5)**

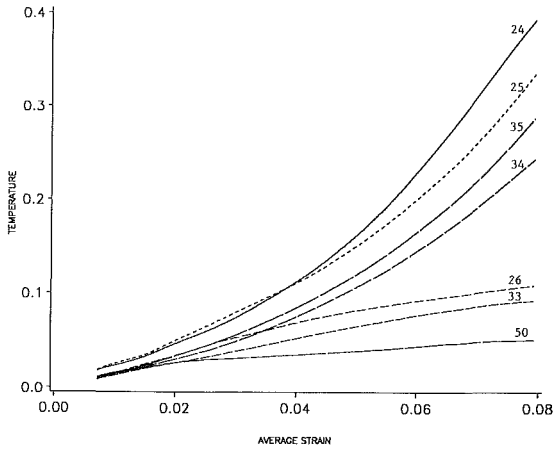

Fig. 6*(b)* **Evolution of θ at matrix points 24, 25, 26, 33, 34, 35 near the matrix/layer interfaces and point 50 in the matrix when $\sigma_0^{layer} = 0.2\,\sigma_0^{matrix}$.**

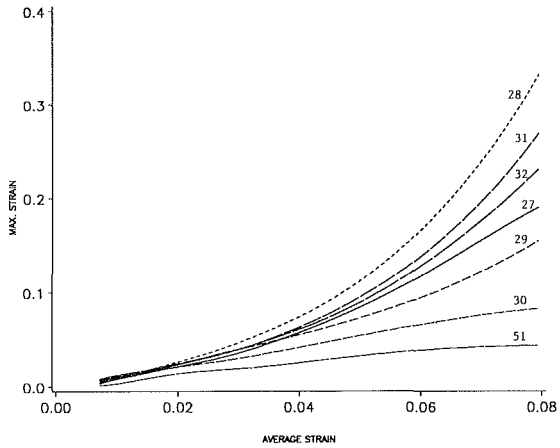

Fig. 6*(c)* **Evolution of ϵ at layer points 27, 28, 29, 30, 31, 32 and 51 near the matrix/layer interfaces when $\sigma_0^{layer} = 0.2\,\sigma_0^{matrix}$.**

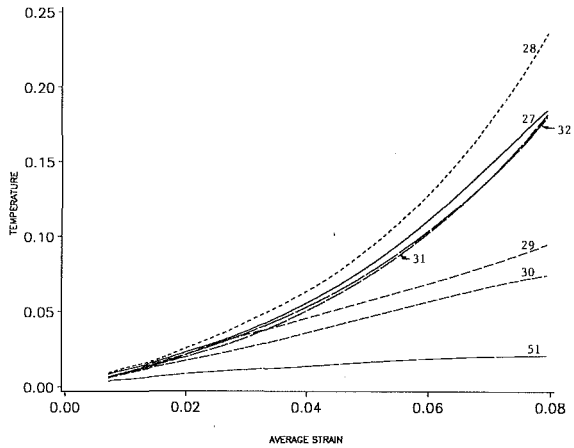

Fig. 6*(d)* **Evolution of θ at layer points 27, 28, 29, 30, 31, 32 and 51 near the matrix/layer interfaces when $\sigma_0^{layer} = 0.2\,\sigma_0^{matrix}$.**

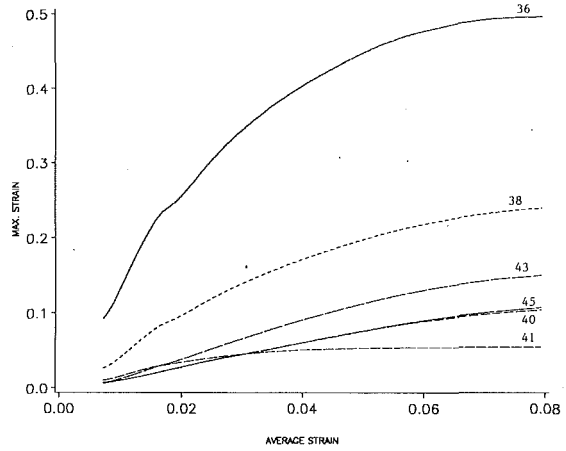

Fig. 7*(a)* Evolution of ϵ at layer points 36, 38 and 40, and matrix points 41, 43 and 45 near the upper matrix/layer interface when $\sigma_0^{layer} = 0.2\ \sigma_0^{matrix}$.

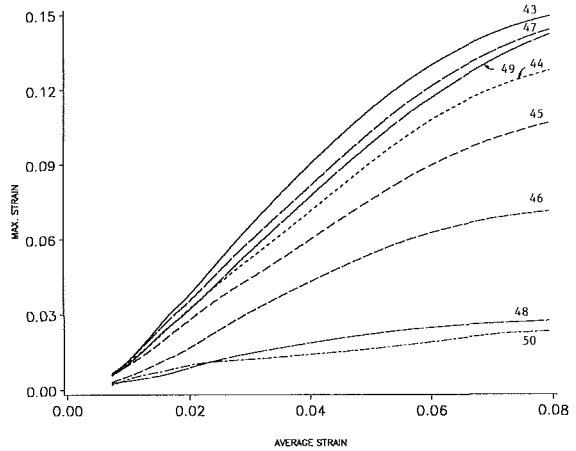

Fig. 7*(b)* Evolution of ϵ at matrix points 43, 44, 45, 46, 47, 48, 49 and 50 when $\sigma_0^{layer} = 0.2\ \sigma_0^{matrix}$.

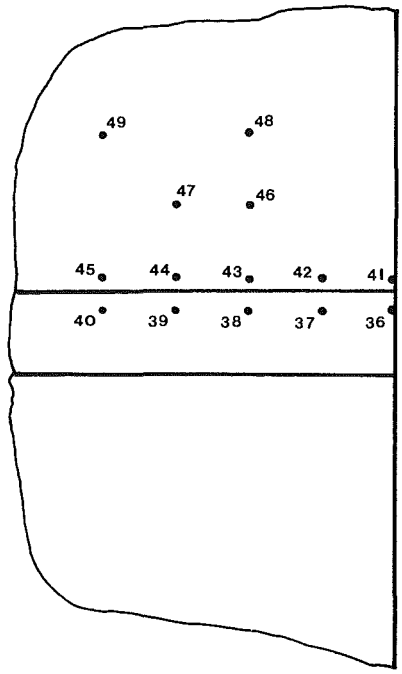

Fig. 7*(c)* Approximate location of points where the evolution of ϵ is plotted in Figs. 7*(a)* and 7*(b)*. The coordinates of these points are: 36(0.9999, 0.515), 38(0.91, 0.515), 40(0.82, 0.515), 41(0.9999, 0.535), 43(0.91, 0.535), 45(0.82, 0.535), 46(0.91, 0.58), 47(0.865, 0.58), 48(0.91, 0.625), 49(0.82, 0.625).

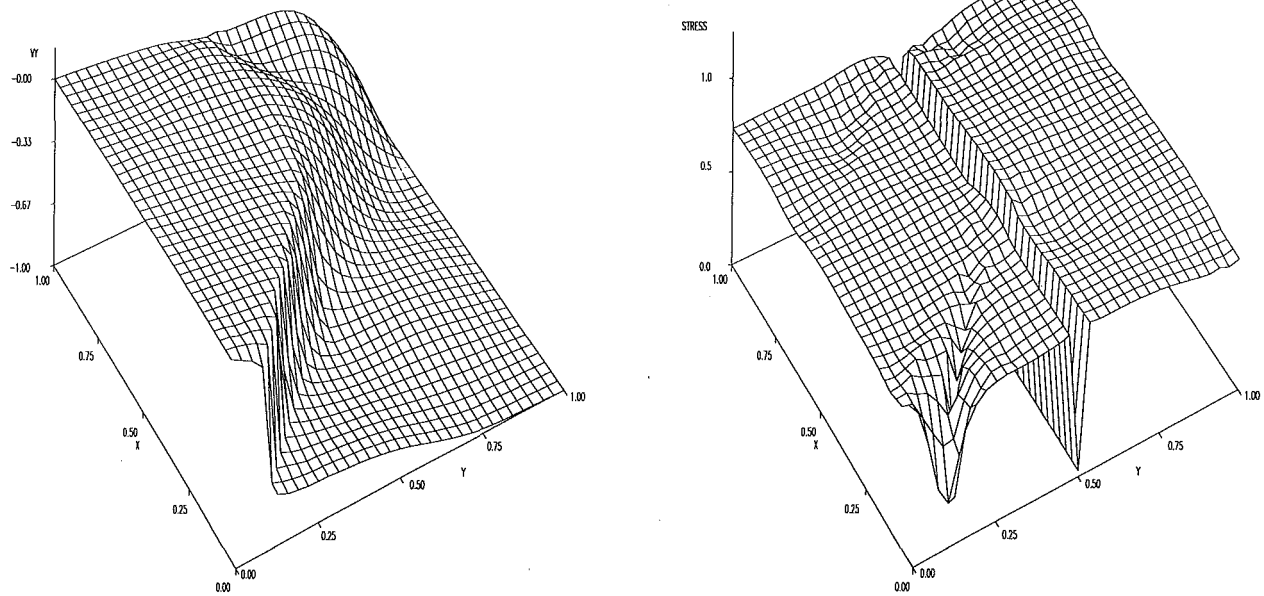

Fig. 8 Distribution of v_2 and the effective stress when $\gamma_{avg} = 0.0601$ and σ_0^{layer} and $0.2\ \sigma_0^{matrix}$.

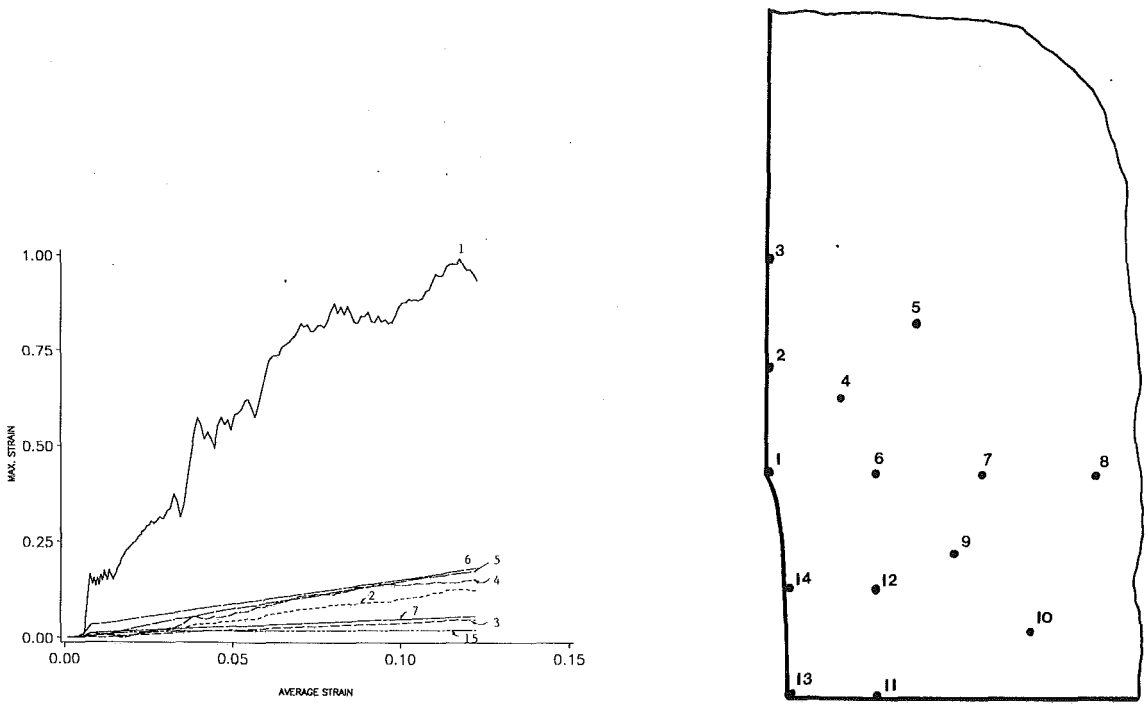

Fig. 9*(a)* **Evolution of ϵ at points 1 through 7 near the void tip and point 15 in the matrix when $\sigma_0^{layer} = 5\ \sigma_0^{matrix}$. Also shown is the approximate location of points 1 through 12 where the evolution of ϵ and θ is plotted in Figs. 9*(a)* through 9*(d)*. The coordinates of these points and point 15 are: 1(0.1 E-04, 0.1), 2(0.1 E-04, 0.15), 3(0.1 E-04, 0.2), 4(0.0354, 0.1354), 5(0.0707, 0.1707), 6(0.05, 0.1), 7(0.1, 0.1), 8(0.15, 0.1), 9(0.0854, 0.0646), 10(0.1207, 0.0293), 11(0.05, 0.1 E-04), 12(0.05, 0.05), 15(0.85, 0.1 E-04).**

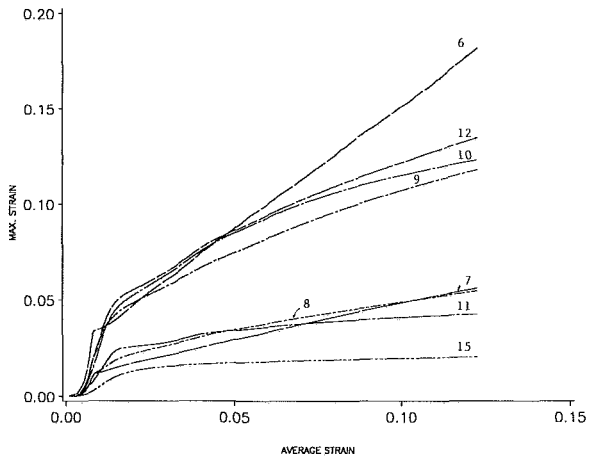

Fig. 9*(b)* **Evolution of ϵ at points 6 through 12 near the void tip and point 15 in the matrix when $\sigma_0^{layer} = 5\ \sigma_0^{matrix}$.**

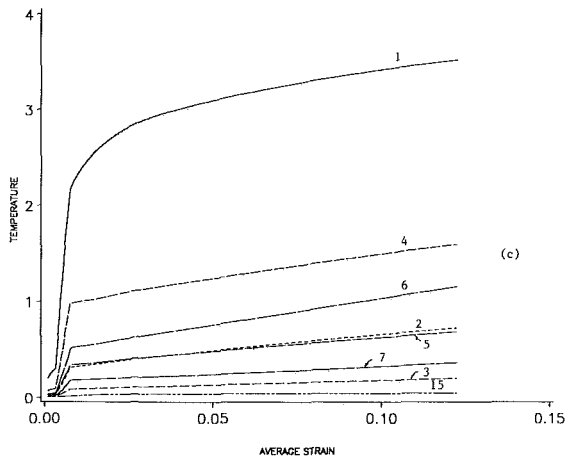

Fig. 9*(c)* **Evolution of θ at points 1 through 7 near the void tip and point 15 in the matrix when $\sigma_0^{layer} = 5\ \sigma_0^{matrix}$.**

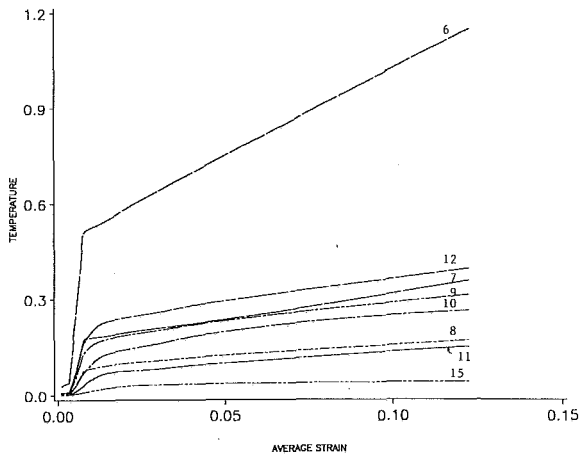

Fig. 9*(d)* **Evolution of θ at points 6 through 12 near the void tip and point 15 in the matrix when $\sigma_0^{layer} = 5\ \sigma_0^{matrix}$.**

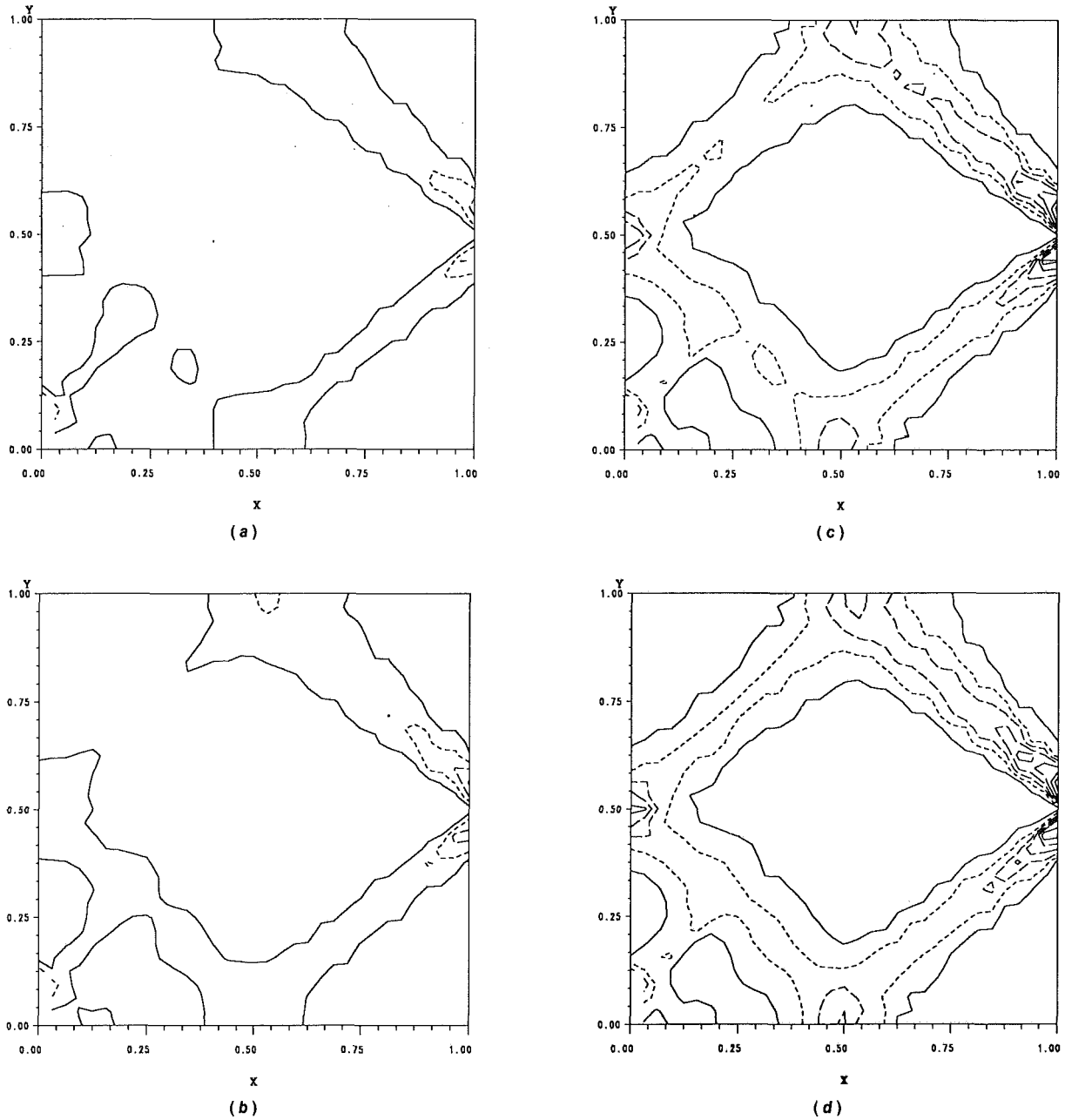

Fig. 10 Contours of the maximum principal logarithmic strain ϵ when $\sigma_0^{layer} = 5\ \sigma_0^{matrix}$ at different values of the average strain. *(a)* $\gamma_{avg} = 0.069$, *(b)* $\gamma_{avg} = 0.076$, *(c)* $\gamma_{avg} = 0.116$, *(d)* $\gamma_{avg} = 0.122$

4.2 Layer Material Stronger than the Matrix Material. We now discuss results for the case when the yield stress in a quasistatic compression test for the layer material equals five times that for the matrix material. Figures 9(*a*) and 9(*b*) depict the evolution of ϵ, and Figs. 9(*c*) and 9(*d*) of θ at 12 points in the vicinity of the ellipsoidal void and also at point 15 in the matrix that is far removed from the void and the matrix/layer interfaces. The approximate location of these points, except for point 15, is shown in Fig. 9(*a*) and their coordinates are given in the caption to that figure. In sharp contrast to the previous case, an intense shear band now initiates from point 1 near the void tip. Since the values of ϵ at points 4, 5, and 6 are nearly the same, it is reasonable to conclude that severe deformations at point 1 propagate towards point 6, and also along the line joining points 1, 4, and 5. The temperature rise at point 1 is quite rapid in the beginning but rather gradual afterwards. It seems that the band from point 6 propagates downward toward points 9 and 10 rather than horizontally along the line joining points 1, 6, 7, and 8. Both the temperature rise and the values of ϵ at point 15 remain small, and much lower than the average strain. The contours of ϵ plotted in Figs. 10(*a*) through 10(*d*) for four different values of the average strain support the above picture and also suggest that shear bands initiating from points on the right traction free edge where the matrix/layer interfaces intersect it propagate into the matrix material along lines making an angle of approximately ± 45 deg with the horizontal. The evolution of ϵ plotted in Figs. 11(*a*) through 11(*d*) corroborates this since the large values of ϵ at points 16 and 29 indicate the initiation of bands at these points. Even though the deformations of point 17 are large, those of point 18 vertically above it are quite small. Also the deformations of the material at points 21 and 22 are miniscule as compared to those of the material at points 16 and 17. Since the layer material is stronger, its deformations are quite a bit smaller than those of adjoining matrix points. However, the stress at the layer points is rather

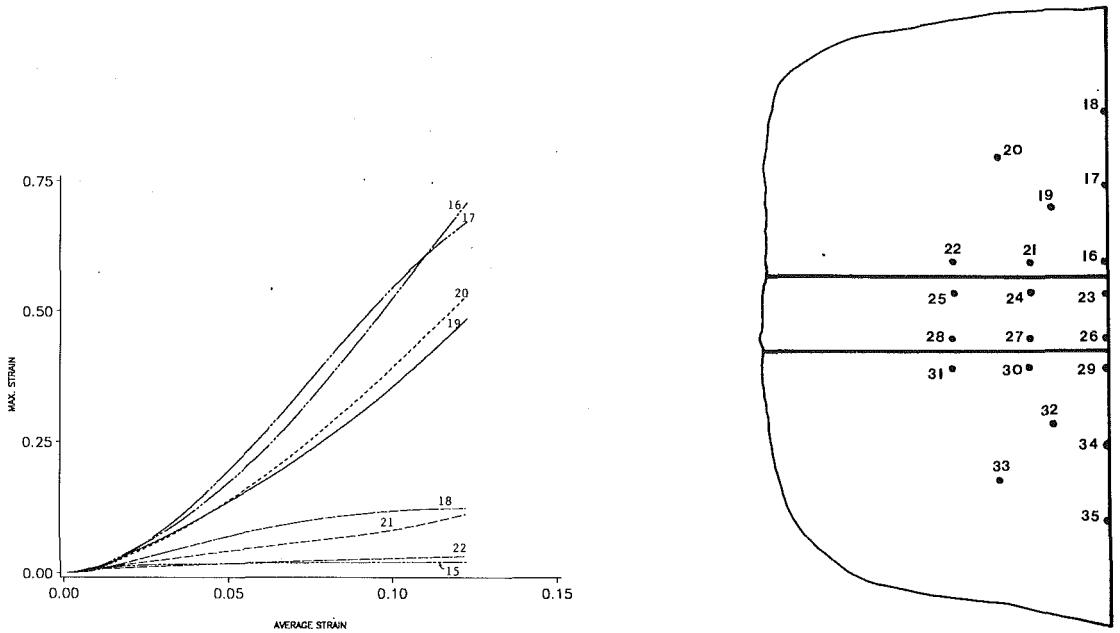

Fig. 11*(a)* **Evolution of ϵ at matrix points 16 through 21 near the upper matrix/layer interface and point 15 in the matrix when $\sigma_0^{layer} = 5\ \sigma_0^{matrix}$. The insert shows the approximate location of points where the evolution of ϵ is plotted in Figs. 11*(a)* through 11*(d)*. The coordinates of these points are: 15(0.85, 0.1 E-04), 16(0.9999, 0.535), 17(0.9999, 0.585), 18(0.9999, 0.635), 19(0.965, 0.57), 20(0.9293, 0.606), 21(0.95, 0.535), 22(0.9, 0.535), 23(0.9999, 0.515), 24(0.95, 0.515), 25(0.9, 0.515), 26(0.9999, 0.485), 27(0.95, 0.485), 28(0.9, 0.485), 29(0.0000, 0.465), 31(0.9, 0.465), 32(0.965, 0.4296), 34(0.9999, 0.415), 35(0.9999, 0.365).**

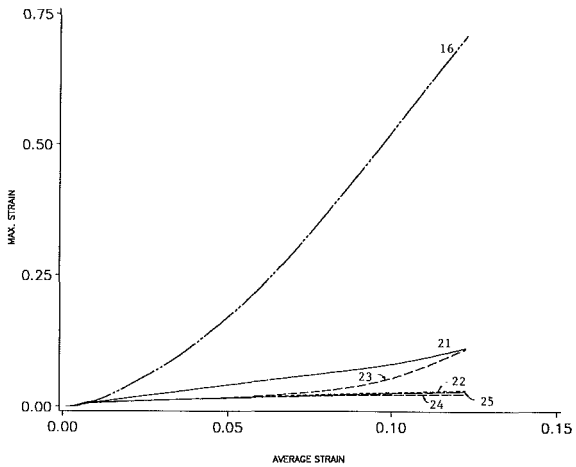

Fig. 11*(b)* **Evolution of ϵ at matrix points 16, 21 and 22, and layer points 23, 24 and 25 near the upper matrix/layer interface when $\sigma_0^{layer} = 5\ \sigma_0^{matrix}$.**

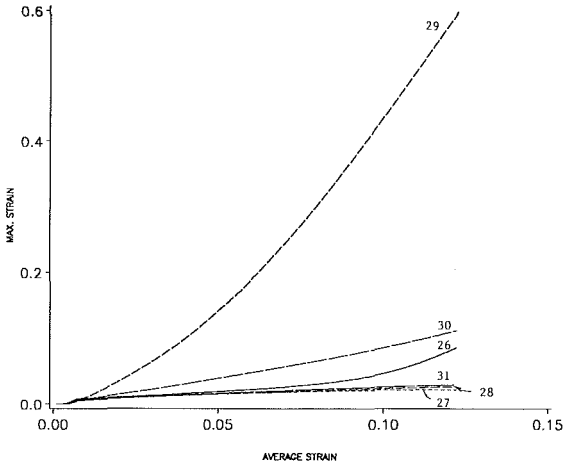

Fig. 11*(c)* **Evolution of ϵ at layer points 26, 27 and 28 and matrix points 29, 30 and 31 near the matrix/layer interface when $\sigma_0^{layer} = 5\ \sigma_0^{matrix}$.**

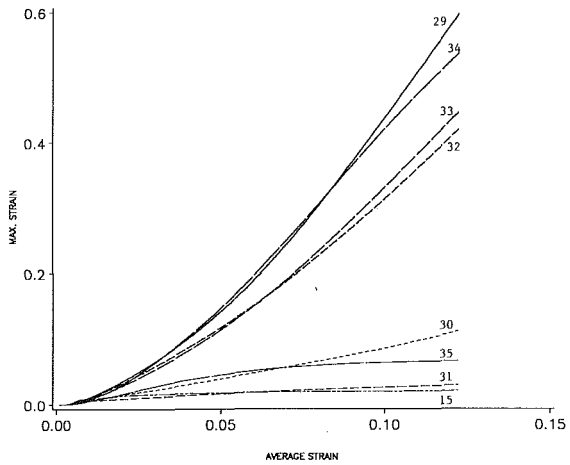

Fig. 11*(d)* **Evolution of ϵ at matrix points 29 through 35 near the matrix/layer interface when $\sigma_0^{layer} = 5\ \sigma_0^{matrix}$. The plots at other points are shown for comparison purposes.**

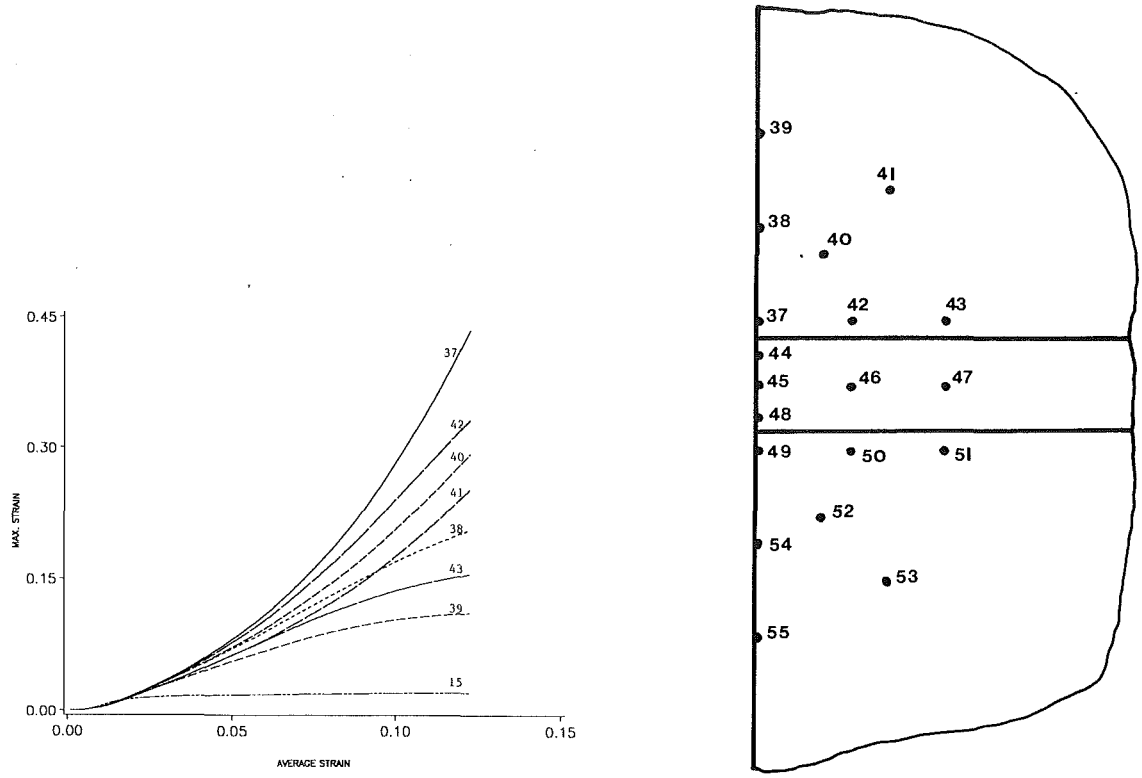

Fig. 12(a) Evolution of ϵ at matrix points 37 through 43 near the vertical centroidal axis and the matrix/layer interface when $\sigma_0^{layer} = 5\ \sigma_0^{matrix}$. Also shown are the approximate location of points where the evolution of ϵ is plotted in Figs. 12(a) through 12(c). The coordinates of these points are: 36(0.5, 0.5), 37(0.1 E-04, 0.535), 38(0.1 E-04, 0.585), 39(0.1, 0.635), 40(0.0354, 0.57), 41(0.0707, 0.606), 42(0.05, 0.535), 43(0.1, 0.535), 44(0.1 E-04, 0.515), 45(0.1 E-04, 0.5), 46(0.05, 0.5), 47(0.1, 0.5), 48(0.1 E-04, 0.485), 49(0.1 E-04, 0.465), 50(0.05, 0.465), 51(0.1, 0.465), 52(0.0354, 0.4296), 53(0.0707, 0.3943), 54(0.1 E-04, 0.415), 55(0.1 E-04, 0.365).

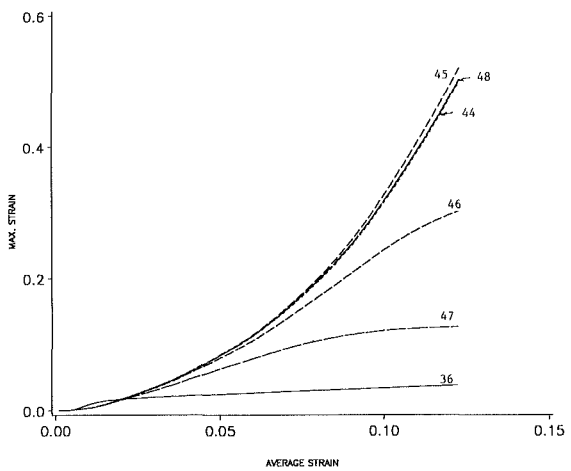

Fig. 12(b) Evolution of ϵ at layer points 44 through 48 near the vertical centroidal axis and the matrix/layer interface when $\sigma_0^{layer} = 5\ \sigma_0^{matrix}$. The evaluation of ϵ at the layer point 36 which is near the center of the analyzed region is shown for comparison purposes.

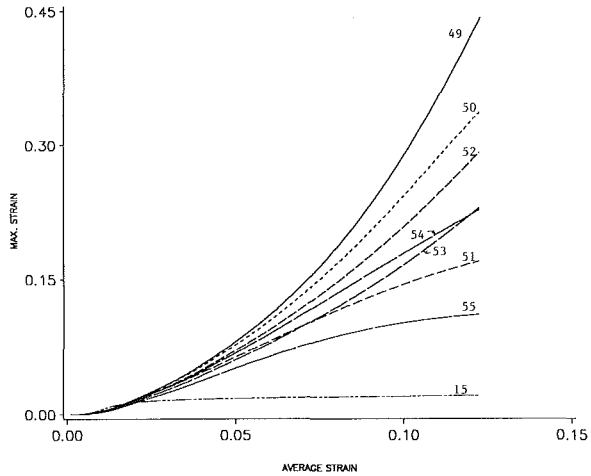

Fig. 12(c) Evolution of ϵ at matrix points 49 through 55 near the vertical centroidal axis and the matrix/layer interface when $\sigma_0^{layer} = 5\ \sigma_0^{matrix}$. The evolution of ϵ at the matrix point 15 which is far removed from the void tip and the matrix/layer interfaces is shown for comparison purposes.

large and thus the resulting temperature rise there may be comparable to that at the corresponding matrix points. The development of ϵ at points near the lower matrix/layer interface is analogous to that at points near the upper matrix/layer interface. Thus shear bands initiating from points 16 and 29 on the matrix/layer interfaces propagate into the matrix material along lines joining points 16, 19, 20, and 29, 32, 33, respectively. These lines make angles of approximately ± 45 deg with the horizontal.

The contours of ϵ plotted in Fig. 10(*e*) suggest that the layer material near points F and G on the left edge of the material in the first quadrant may have undergone severe deformations too. Accordingly, we have plotted in Figs. 12(*a*) through 12(*c*) the evolution of ϵ at several points near the matrix/layer interfaces and the left edge of the region analyzed. The approximate location of these points is shown in Fig. 12(*a*) and their coordinates are given in the figure caption. The values of ϵ at points 44, 45, and 48 in the layer are comparable to those at points 49, 50, 52, 37, 40, 41, and 42 in the matrix. One reason for the significant deformations of these layer points is that two bands, one initiating from the mirror image Q^* through x_1-axis of point Q and the other from point Q^{**}, the mirror image of Q^* through x_2-axis, intersect there. Even though the layer material is harder, the temperature θ at points

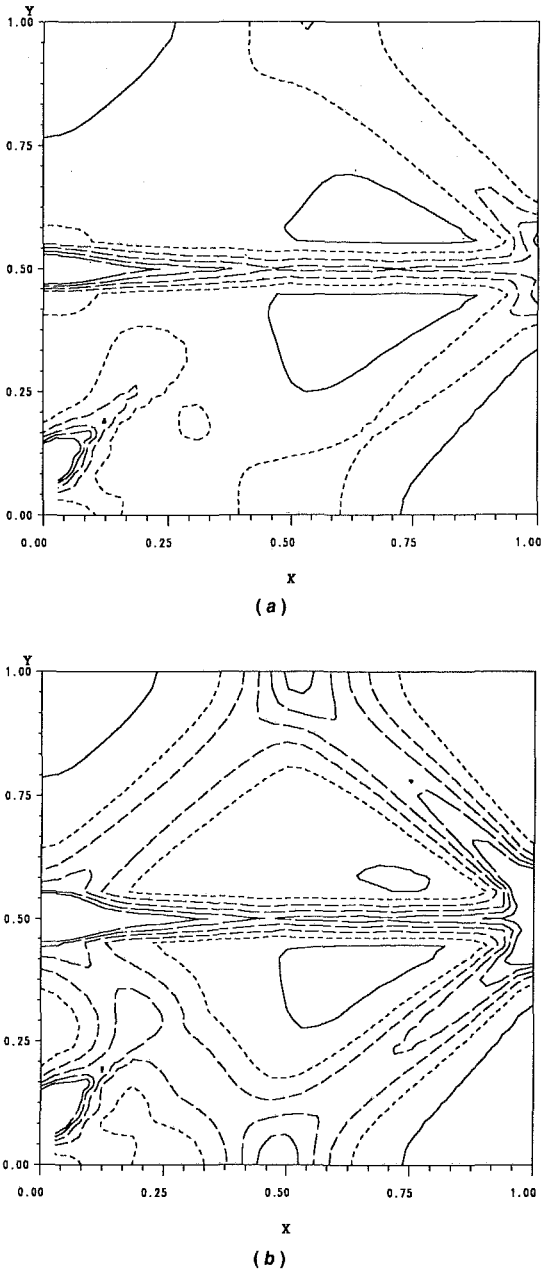

Fig. 13 Contours of the temperature rise θ *(a)* $\gamma_{avg} = 0.069$, *(b)* $\gamma_{avg} = 0.122$ when $\sigma_0^{layer} = 5\ \sigma_0^{matrix}$.

44, 45, and 48 has risen enough to soften it and facilitate its large deformations. The contours of θ at two different values of the average strain are shown in Fig. 13. A reason for noticeable temperature rise of the layer particles is that the stress there is quite high thus resulting in significant plastic working even for small deformations of the layer material.

The distribution of the vertical component v_2 of the velocity field at an average strain of 0.122 is shown in Fig. 14. It is clear that the region analyzed is divided into five subregions, each of which is deforming essentially rigidly and there is a sharp jump in the value of v_2 across boundaries separating these regions. In this case, the band initiating from the void tip is not very intense.

Conclusions

We have analyzed the problem of the initiation and growth of shear bands in a prismatic viscoplastic body of square cross-section containing an ellipsoidal void with major axis aligned

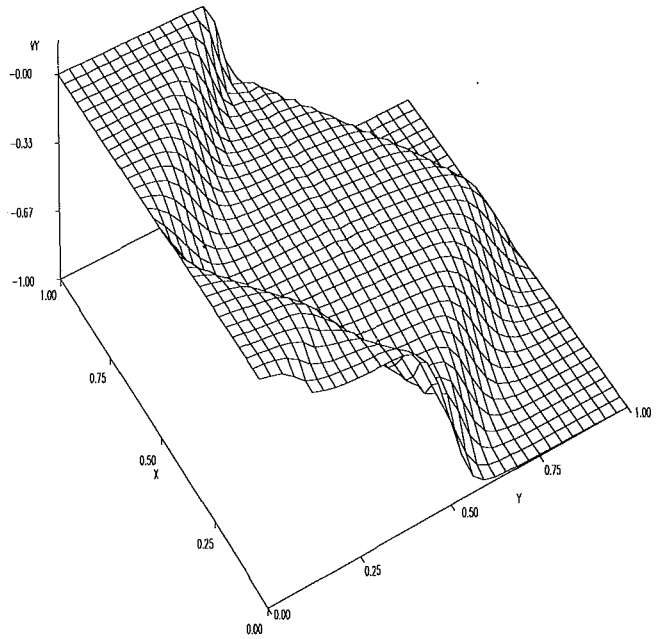

Fig. 14 Distribution of the vertical component v_2 of the velocity at $\gamma_{avg} = 0.122$ when $\sigma_0^{layer} = 5\ \sigma_0^{matrix}$.

along the vertical centroidal axis and two thin layers made of a different viscoplastic material placed symmetrically about the horizontal centroidal axis. The body is deformed in plane strain compression along the vertical axis at a nominal strain-rate of 5000 s^{-1}, and its deformations are assumed to be symmetrical about the two centroidal axes. The deformations of the material in the first quadrant have been analyzed.

When the layer material is softer than the matrix material, it is found that a shear band emerges from a point slightly away from the void tip and propagates along the direction of the maximum shear stress. It passes through the layer rather easily. Shear bands also initiate from points on the traction free edge where the matrix/layer interfaces intersect it. These bands initially propagate as one band horizontally into the layer. Subsequently, it bifurcates into two bands each one of which propagates into the matrix material along lines making an angle of ± 45 deg with the horizontal. There is not much interaction between these bands and the one initiating from a point a bit away from the void tip. However, when the layer material is harder than the matrix material a shear band initiates from a point adjacent to the void tip. Shear bands originating from points of intersection of the traction free edge and the matrix/layer interfaces propagate into the matrix material along lines making an angle of ± 45 deg with the horizontal. There is a strong interaction between these bands and those initiating from points adjacent to the void tips, and the latter do not arrive at the matrix/layer interface and are deflected. Eventually, the region in the quadrant analyzed is divided into five subregions, each one of which is deforming rigidly and the velocity field suffers a sharp jump across the boundaries between these regions.

Acknowledgments

This work was supported by the National Science Foundation grant MSM 8715952 and the U.S. Army Research Office Contract DAAL03-88-K-0184 to the University of Missouri-Rolla.

References

Anand, L., Lush, A. M., and Kim, K. H., 1988, "Thermal Aspects of Shear Localization in Viscoplastic Solids," *Thermal Aspects in Manufacturing*, M. H. Attia and L. Kops., ed., ASME-PED Vol. 30, pp. 89–103.

Bathe, K. J., 1982, *Finite Element Procedures in Engineering Analysis*, Prentice-Hall, Englewood Cliffs, NJ.

Batra, R. C. and Kim, C. H., 1990a, "Effect of Viscoplastic Flow Rules on the Initiation and Growth of Shear Bands at High Strain Rates," *J. Mechs. Phys. Solids* (in press).

Batra, R. C. and Kim, C. H., 1990b, "Adiabatic Shear Banding in Elastic-Viscoplastic Nonpolar and Dipolar Materials," *Int. J. Plasticity*, Vol. 6, pp. 127–141.

Batra, R. C. and Liu, D. S., 1990, "Adiabatic Shear Banding in Dynamic Plane Strain Compression of a Viscoplastic Material," *Int. J. Plasticity*, Vol. 6, pp. 231–246.

Batra, R. C. and Liu, D. S., 1989, "Adiabatic Shear Banding in Plane Strain Problems," ASME *Journal of Applied Mechanics*, Vol. 56, pp. 527–534.

Batra, R. C. and Zhang, X. T., 1990, "Shear Band Development in Dynamic Loading of a Viscoplastic Cylinder Containing Two Voids," *Acta Mechanica*, Vol. 85, pp. 221–234.

Batra, R. C. and Zhu, Z. G., 1990, "Dynamic Shear Band Development in a Thermally Softening Bimetallic Body Containing Two Voids," *Acta Mechanica*, Vol. 86, pp. 31–52.

Clifton, R. J., 1980, "Adiabatic Shear Banding," in Material Response to Ultrahigh Loading Rates, Chapter 8, NRC National Material Advisory Board (U.S.) Report No. NMAB-356, pp. 129–142.

Dodd, B. and Bai, Y., 1987, *Ductile Fracture and Ductility*, Academic Press, New York.

Gear, C. W., 1971, *Numerical Initial Value Problems in Ordinary Differential Equations*, Prentice-Hall, Englewood Cliffs, NJ.

Hindmarsh, A. C., 1983, "ODEPACK, A Systematized Collection of ODE Solvers," *Scientific Computing*, R. S. Stepleman et al. eds., North-Holland, Amsterdam, pp. 55–64.

Johnson, W., 1987, "Henri Tresca as the Originator of Adiabatic Heat Lines," *Int. J. Mech. Sci.*, Vol. 29, pp. 301–310.

Le Monds, J. and Needleman, A., 1986, "An Analysis of Shear Band Development Incorporating Heat Conduction," *Mech. Mat.*, Vol. 5, pp. 363–373.

LeMonds, J. and Needleman, A., 1986, "Finite Element Analyses of Shear Localization in Rate and Temperature Dependent Solids," *Mech. Mat.*, Vol. 5, pp. 339–361.

Marchand, A. and Duffy, J., 1988, "An Experimental Study of the Formation Process of Adiabatic Shear Bands in a Structural Steel," *J. Mechs. Phys. Solids*, Vol. 36, pp. 251–283.

Marchand, A., Cho, K., and Duffy, J., 1988, "The Formation of Adiabatic Shear Bands in an AISI 1018 Cold-Rolled Steel," Brown Univ. Report.

Massey, H. F., 1921, "The Flow of Metal During Forging," *Proc. Manchester Assoc. Engineers*, pp. 21–26.

Needleman, A., 1989, "Dynamic Shear Band Development in Plane Strain," ASME *Journal of Applied Mechanics*, Vol. 59, pp. 1–9.

Needleman, A. and Tvergaard, V., 1984, "Finite Element Analysis of Localization in Plasticity," *Finite Elements: Special Problems in Solid Mechanics*, J. T. Oden and G. F. Carey, eds., pp. 94–157.

Recht, R. F., 1964, "Catastrophic Thermoplastic Shear," ASME *Journal of Applied Mechanics*, Vol. 31, pp. 189–193.

Semiatin, S. L. and Jonas, J. J., 1984, *Formability and Workability of Metals: Plastic Instability and Flow Localization*, ASM, Metals Park.

Shawki, T. G. and Clifton, R. J., 1989, "Shear Band Formation in Thermal Viscoplastic Materials," *Mech. Mat.*, Vol. 8, pp. 13–43.

Tresca, H., 1878, "On Further Application of the Flow of Solids," *Proc. Inst. Mech. Engr.*, Vol. 30, pp. 301–345.

Wulf, G. L., 1978, "The High Strain Rate Compression of 7039 Aluminum," *Int. J. Mech.*, Vol. 20, pp. 609–615.

Zbib, H. M. and Aifantis, E. C., 1988, "On the Localization and Postlocalization Behavior of Plastic Deformation. I., On the Initiation of Shear Bands," *Res. Mechanica*, Vol. 23, pp. 261–277.

Zener, C. and Hollomon, J. H., 1944, "Effect of Strain Rate on Plastic Flow of Steel," *J. Appl. Phys.*, Vol. 14, pp. 22–32.

Zhu, Z. G. and Batra, R. C., 1990, "Dynamic Shear Band Development in Plane Strain Compression of a Viscoplastic Body Containing a Rigid Inclusion," *Acta Mechanica* , Vol. 84, pp. 89–107.

Zhu, Z. G. and Batra, R. C., 1991, "Shear Band Development in a Thermally Softening Viscoplastic Body," *Computers and Structures* (in press).